2. Observing through the atmosphere

The main limitation of observing from the ground is the atmospheric absorption, variable opacity of the atmosphere, and the background infrared emission.

2.1 Atmospheric transmission

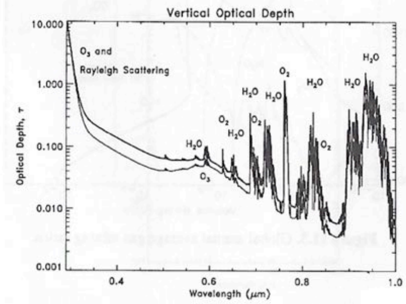

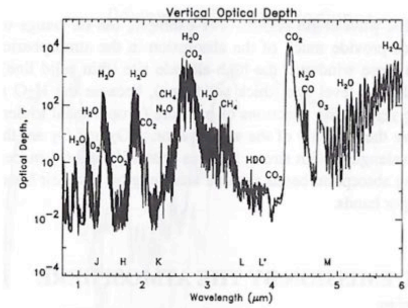

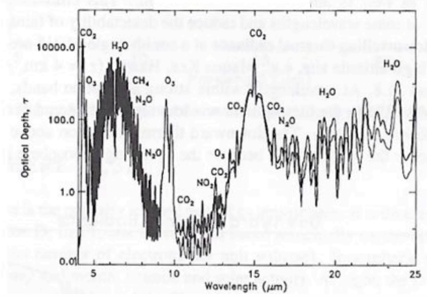

Optical depth looking at zenith, from Crisp (2000). The atmospheric transmission is $e^{-\tau}$, where τ is the optical depth.

This slide shows the optical depth of major atmospheric absorbers in the visible and infrared. Note that the optical depth is much greater in the infrared due to the strong molecular fundamental absorption bands in the infrared. Figures are from Crisp, D. (2000).

High spectral resolution overview of the atmospheric transmission (Smette et al. 2015). Note that water is the main absorber, followed by carbon dioxide. Ozone is a strong absorber in 9.5 μm.

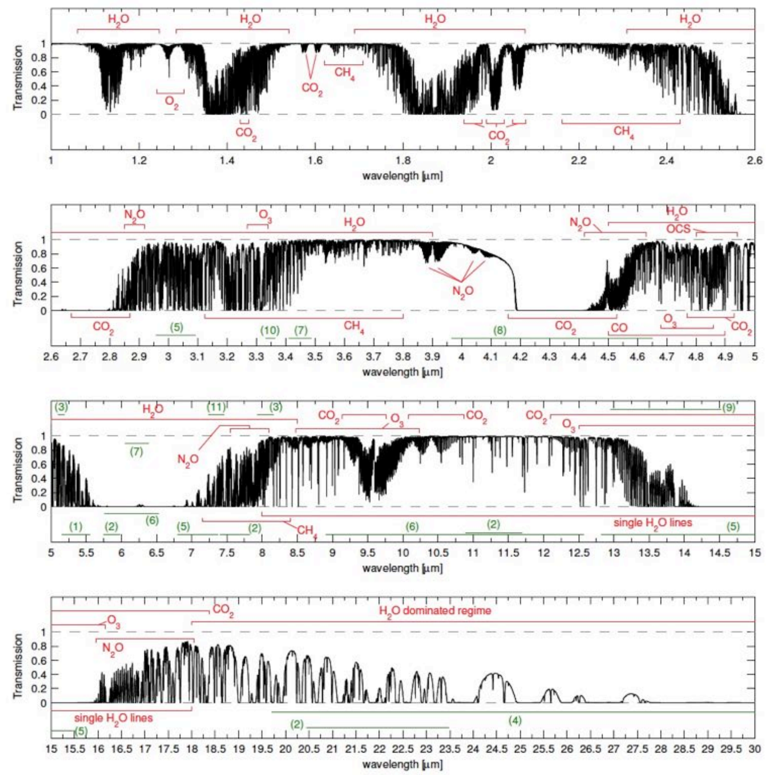

From: Smette, A. et al. (2015). "Molecfit: A general tool for telluric absorption correction. I. Method and application to ESO instruments." Astronomy and Astrophysics **576**.

Ground-based atmospheric windows.

Most of the ground-based observing is done at 1-20 μm. The atmospheric windows is shown below for the summit of Maunakea (Tokunaga 2000).

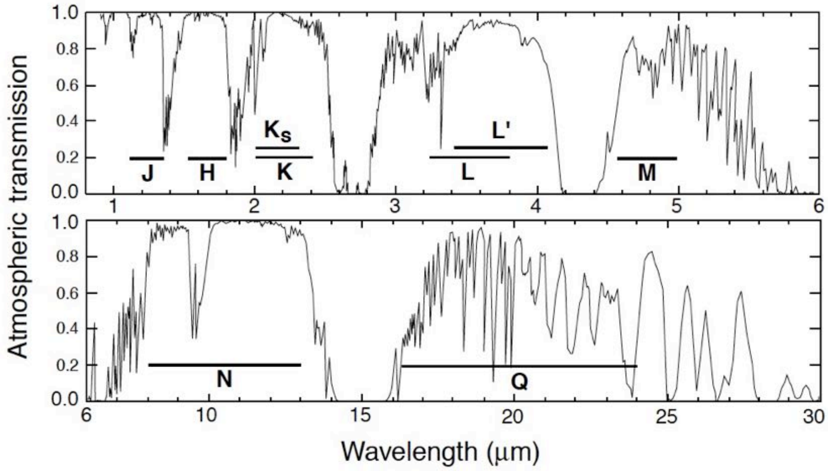

A high resolution calculation of the atmospheric transmission is shown at:

http://www.gemini.edu/sciops/telescopes-and-sites/observing-condition-constraints/ir-transmission-spectra

A. Tokunaga, Introduction to Infrared Astronomy, Feb. 2018

2- 3

Figure is from: Tokunaga, A. T. (2000). Infrared Astronomy. Allen's Astrophysical Quantities, 4th edition. A. N. Cox. New York, Springer-Verlag**:** 143.

The high transparency regions of the atmosphere are called atmospheric windows and are labeled as J, H, K, L, M, N, and Q following Johnson, H. L. (1966). "Astronomical Measurements in the Infrared." Annual Review of Astronomy and Astrophysics **4**: 193. Johnson's filters were very broad and the figure above shows the modern filter bandpass as horizontal bars. These filters are much more narrow than Johnson's filters to provide more precise photometry and better color transformation between observatories.

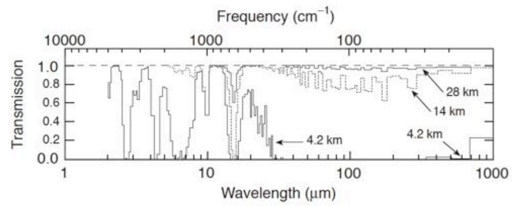

Low-resolution atmospheric transmission from 1-1,000 μm at different altitudes. The altitude of Maunakea is 4.2 km. The SOFIA airborne observatory flies at 14 km. Balloon observatories fly at 28 km or higher.

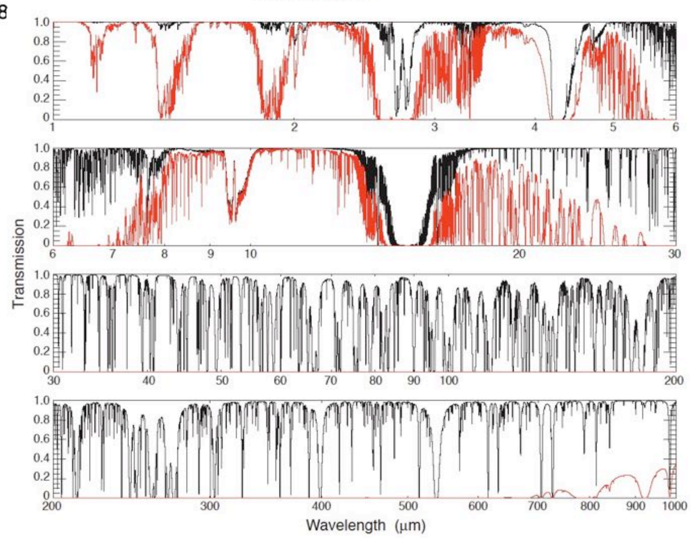

High-resolution atmospheric transmission from 1-1,000 μm. The red line shows the atmospheric transmission at Maunakea [precipitable water (PWV) =3.4mm]. The black line shows atmospheric transmission for SOFIA flying at 12.5 km (PWV =7.3 μm).

Upper figure is from: Traub, W. A. and M. T. Stier (1976). "Theoretical atmospheric transmission in the mid- and far-infrared at four altitudes." Applied Optics **15**: 364-377.
Lower figure is from: Tokunaga, A. T., W. D. Vacca and E. T. Young (2013). Infrared Astronomy Fundamentals. Planets, Stars and Stellar Systems. Vol. 2, Astronomical Techniques, Software, and Data. T. D. Oswalt and H. E. Bond. Dordrecht, Springer Science+Business Media, 99-174.

Far-infrared transmission of the atmosphere.

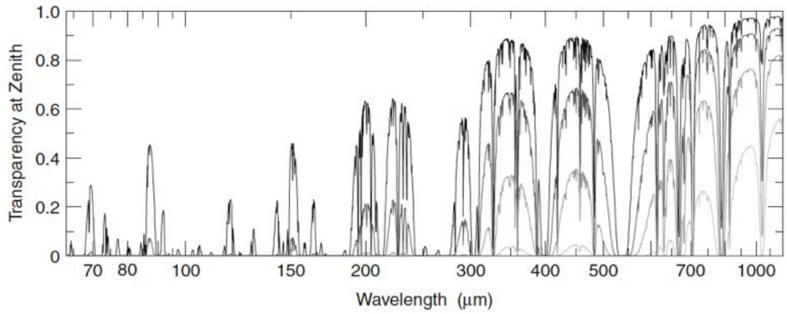

Computed atmospheric transparency at zenith between 70 and 1,000 µm for a site at an altitude of 5,100 m (Llano de Chajnantor) and different H_2O column densities: The tracings, top to bottom, correspond to 0.1, 0.4, 1.0, and 3.0 mm of PWV (Giovanelli et al. 2001).

The typical PWV at this site is 1.2 mm, and this shows that Chajnantor is about three times better than Maunakea at 850 µm.

Giovanelli, R., J. et al. (2001). "The Optical/Infrared Astronomical Quality of High Atacama Sites. II. Infrared Characteristics." Publications of the Astronomical Society of the Pacific **113**: 803-813.

Comparison of the Tokyo Atacama Obs. site to Paranel.

Chajnantor in context to TAO. Cerro Chajnantor in the Atacama desert of northern Chile, with an altitude of 5640m. This figure shows the comparison of Cerro Chajnantor to a typical lower altitude site.

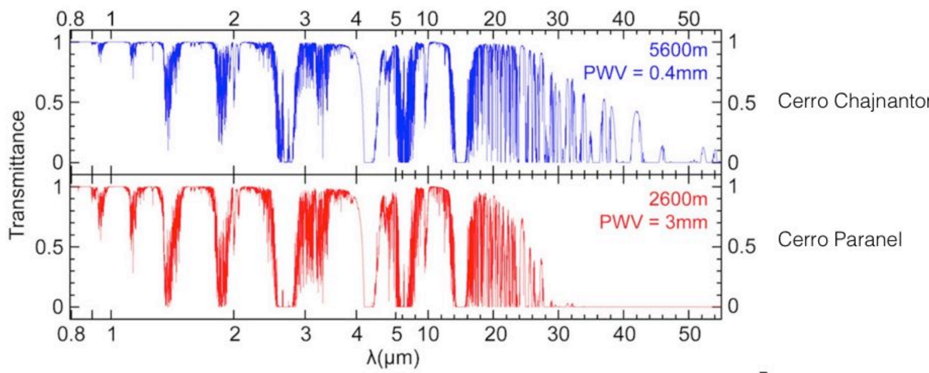

K. Motohara et al. 2016, http://spie.org/newsroom/6796-new-65m-ir-optimized-high-altitude-observatory-in-northern-chile

Comparison of an Antarctic site with Atacama.

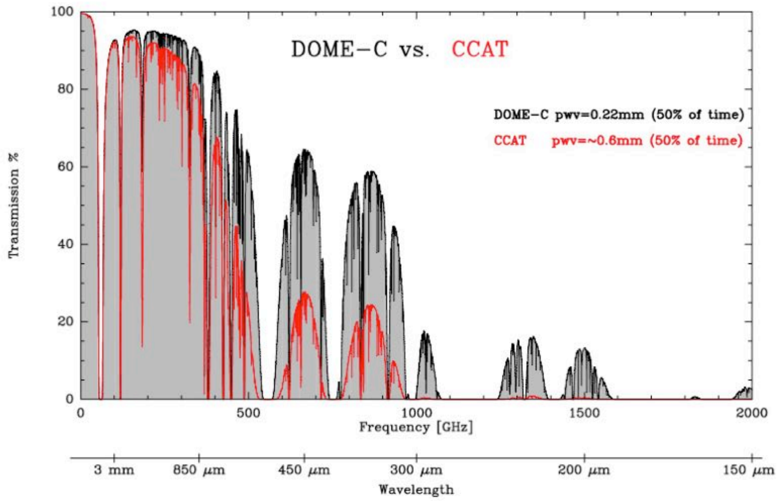

Atmospheric transmission for Dome C at Antarctica and the Cerro Chajnantor Atacama Telescope-prime (CCAT-p) corresponding to 0.22 mm precipitable water vapor (pwv) for Dome C and 0.6 mm pwv for the CCAT-p site (Schneider et al. 2010). Although the Dome C site is at a lower altitude (3200 m) than the CCAT-p site (5600 m), the Dome C site is much colder and therefore has less pwv.

Shows the atmospheric transmission at the 50th percentile, that is 50% of the time the water vapor is smaller than 0.22mm at Dome C and smaller than 0.6mm at the CCAT site.

Schneider, N. et al. (2010). Atmospheric Transmission At Dome C Between 0 AND 10 THz. EAS Publications Series. L. Spinoglio and N. Epchtein. ed., 40: 327-332.

Selected list of high and medium altitude observatories

Site	Altitude (m)	Telescopes
Cerro Chajnantor (Chile)	5600	TAO
Llano de Chajnantor (Chile)	5100	ALMA
Sierra Negra (Mexico)	4800	Large Millimeter Telescope
Mauna Kea (Hawaii)	4200	Keck, Gemini-N, Subaru, CFHT
Mt. Graham (Arizona)	3200	Large Binocular Telescope
Cerro Amazonas (Chile)	3100	E-ELT
Haleakala (Hawaii)	3000	Pan-STARRS, LCOGT
South Pole	2800	South Pole Telescope
Sierra San Pedro Martir (Mexico)	2800	2.1m Telescope
Cerro Pachon (Chile)	2700	Gemini-S, LSST
Cerro Paranel (Chile)	2600	VLT, VISTA
Roque de los Muchachos (La Palma)	2400	GTC, TNG, WHT
La Silla (Chile)	2400	ESO, NTT
Palomar Mountain (California)	1700	Hale Telescope

Source: https://en.wikipedia.org/wiki/List_of_highest_astronomical_observatories

Maunakea Observatories. Major facilities: Keck I and II, Subaru, Gemini North, Canada-France-Hawaii Telescope, East Asia Observatory (formerly JCMT), Sub-millimeter Array, United Kingdom Infrared Telescope, NASA Infrared Telescope Facility, UH 2.2m telescope.

Paranal Observatory.   Major facilities: Very Large Telescope (4 x 8.2m), VISTA Survey Telescope, VLT Survey Telescope, Next Generation Transit Survey.

Roque de los Muchachos Observatory (La Palma). Major facilities: Gran Telescopio Canarias, Galileo National Telescope, Isaac Newton Group of Telescopes, Nordic Optical Telescope, Major Atmospheric Gamma Imaging Cherenkov Telescopes, SuperWASP

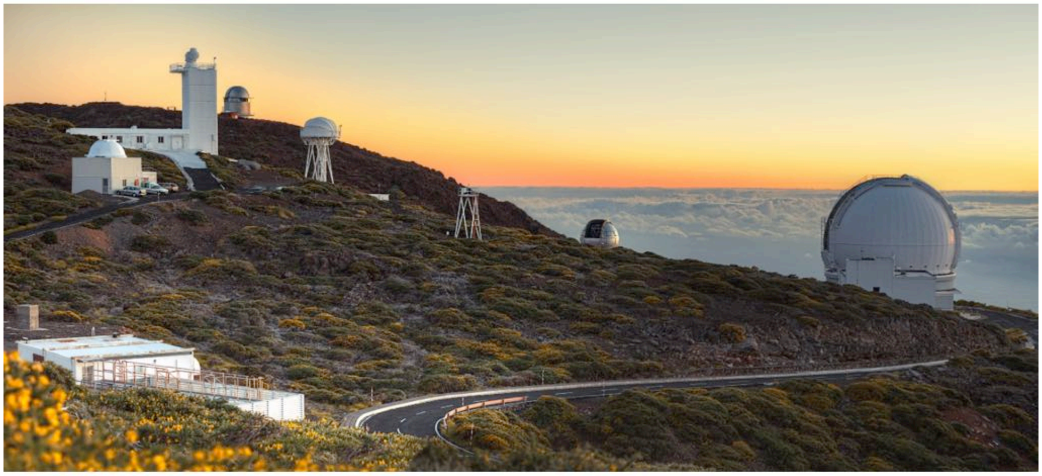

Llano de Chajnantor and Cerro Chajnantor

Image from: https://www.eso.org/public/images/potw1302a/
Show ALMA site in 2013.

Cerro Chajnantor and TAO

2- 13

Image from: https://www.eso.org/public/images/potw1302a/
Show ALMA site in 2013.

Stratospheric Observatory for Infrared Astronomy.   2.5-m telescope in a modfied 747SP aircraft. Operates at an altitude of about 14 km.

Example of high-altitude balloon flown in Antarctica for 22 days.

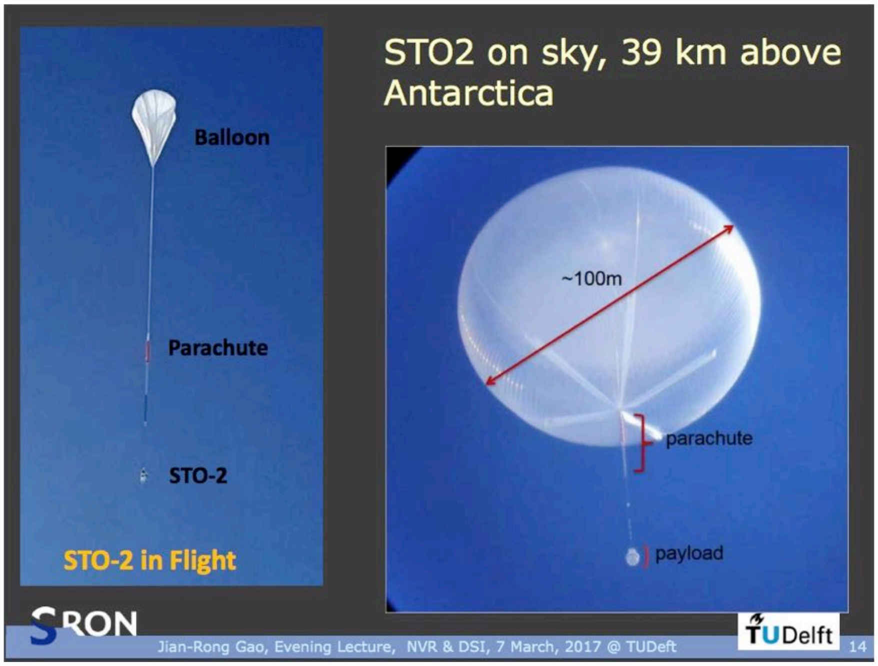

Balloon astronomy might the frontier for the far-IR in the future.
https://www.ruimtevaart-nvr.nl/media/vk_1223/Website/documenten/STO2_NVR_DSI_2017_Presentation.pdf
39 km = 128,000 feet

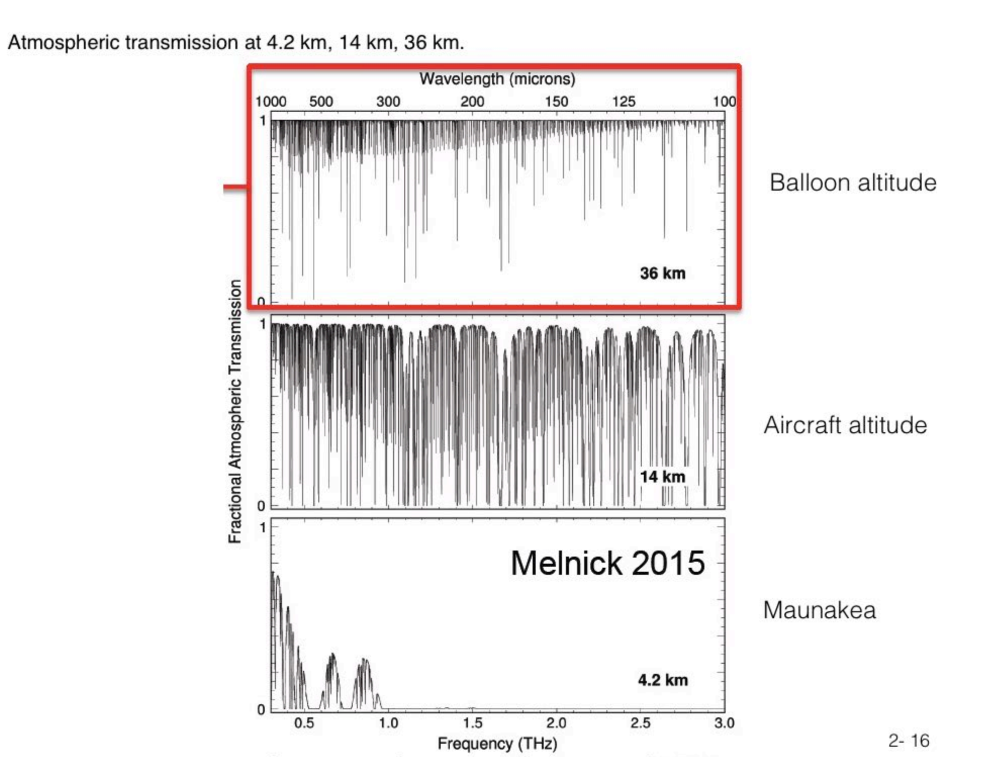

From presentation by Chris Walker on GUSTO project.

Resources for estimating the atmospheric transmission:

ATRAN: https://atran.sofia.usra.edu/cgi-bin/atran/atran.cgi
Software for calculating the atmospheric transmission at any resolving power

Gemini web site:
http://www.gemini.edu/sciops/telescopes-and-sites/observing-condition-constraints/ir-transmission-spectra
Tables giving the atmospheric transmission with a sampling of 0.00002μm in wavelength and a resolution of 0.0004μm

Goddard web site: https://ssed.gsfc.nasa.gov/psg/apps/ishell.php
Provides a simulator for using a high resolutions spectrograph at the IRTF and shows the atmospheric transmission for each order. Computed atmospheric transmission can be downloaded.

2.2 Atmospheric extinction

The atmospheric extinction consists of Rayleigh scattering by molecules, molecular absorption, and aerosol scattering by particulates. (Hayes and Latham1975; Killinger et al. 1995). These are highly dependent on the site, seasonal weather patterns, and natural events such as dust storms and volcanic eruptions. Figure below from Smalley et al. (2007) shows the various extinction components: ozone absorption, scattering by aerosol and small particles, and absorption by atmospheric gases.

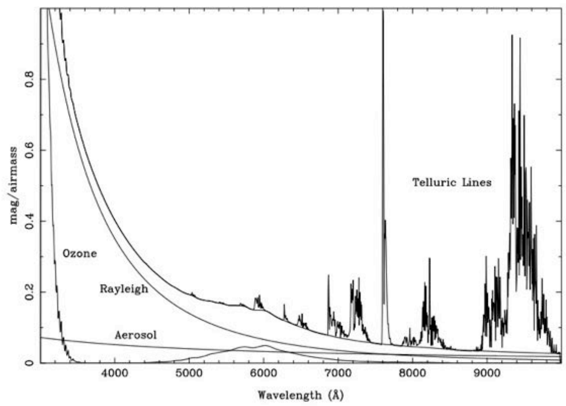

Figure 2. Simulation of the typical extinction by Earth's Atmosphere, showing the relative contributions of Rayleigh and aerosol scattering, ozone and telluric line absorption.

2- 18

Extinction coefficients will be discussed later. This is a measure of the atmospheric extinction in magnitudes as a function of airmass (path length through the atmosphere).

Smalley, B., A. F. Gulliver and S. J. Adelman (2007). The ASTRA Spectrophotometer: Reduction and Flux Calibrations. The Future of Photometric, Spectrophotometric and Polarimetric Standardization. C. Sterken. **364:** 265.

Hayes, D. S. and D. W. Latham (1975). "A rediscussion of the atmospheric extinction and the absolute spectral-energy distribution of Vega." The Astrophysical Journal **197**: 593-601.

Killinger, D. K., J. H. Churnside and L. S. Rothman (1995). Atmospheric Optics. Handbook of Optics. Vol. I. Fundamentals, Techniques, and Design. M. Bass, E. W. V. Stryland, D. R. Williams and W. L. Wolfe. New York, McGraw-Hill, Inc.

Long-term extinction trends show these effects clearly as discussed by Burki et al. (1995) for ESO and Frogel (1998) for CTIO. As emphasized by Frogel, extinction coefficients in the infrared vary considerably because of the effects of water vapor absorption; thus, the extinction coefficient should be measured throughout the night for accurate photometry.

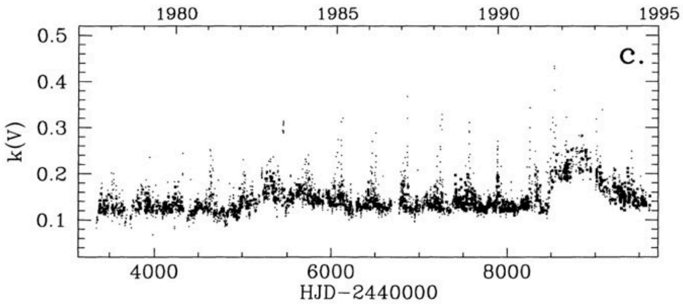

Extinction coefficient in the V-band measured by Burki et al. (1995, figure 3). There are seasonal variations and an increase in 1991 due to the Pinatubo eruption. The need for nightly measurements of the extinction is clear.

Burki, G., et al. (1995). "The atmospheric extinction at the E.S.O. La Silla observatory." Astronomy and Astrophysics Supplement Series **112**: 383.

Frogel, J. A. (1998). "A History of Infrared Extinction at CTIO, Chile, and a Possible Connection with the EL Niño Phenomenon." Publications of the Astronomical Society of the Pacific **110**: 200-209.

See also: Lombardi, G., E. et al. (2011). "A study of NIR atmospheric properties at Paranal Observatory." Astronomy and Astrophysics **528**: 43.

2.3 Atmospheric refraction

The atmosphere of the Earth will refract light and this depends on the refractive index of air. The refractive index of air depends on many parameters: wavelength, atmospheric pressure, partial pressure of water vapor, and temperature. This is discussed in detail by Roe (2002).

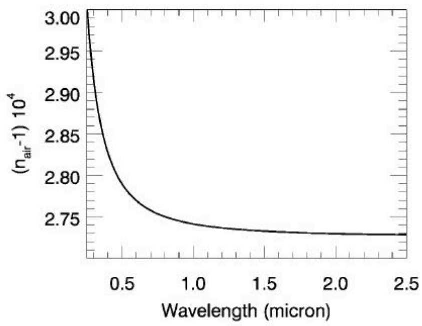

FIG. 2.—Refractive index of air as a function of wavelength across the visible and near-infrared spectrum at standard temperature and pressure in the absence of water vapor.

Figure from Roe (2002) showing the refractive index as a function of wavelength. Note that the refractive index varies greatly at wavelengths less than 1 μm. This shows that the apparent position of an object in the sky may differ at 0.5 μm compared to 2.0 μm, for example, and this is critically important for observing with slit spectrographs or with adaptive optics.

Roe, H. G. (2002). "Implications of Atmospheric Differential Refraction for Adaptive Optics Observations." Publications of the Astronomical Society of the Pacific **114**: 450-461.

See also: Skemer, A. J. (2009). "A Direct Measurement of Atmospheric Dispersion in N-band Spectra: Implications for Mid-IR Systems on ELTs." Publications of the Astronomical Society of the Pacific **121**: 897-904.

The figure below shows the atmospheric dispersion *within* the various filter passbands as a function of zenith distance, the angle between the object being observed and the zenith (from Phillips et al. 2010). This shows, for example, that a point source observed through the J filter would be spread out by about 30 milli-arcsec at an angle of 30° from the zenith. This is significant since the diffraction limit of the Thirty Meter telescope (TMT) is 10 milli-arcsec at J. To minimize the effects of atmospheric dispersion, an atmospheric dispersion corrector is needed as described by Phillips et al. (2010)

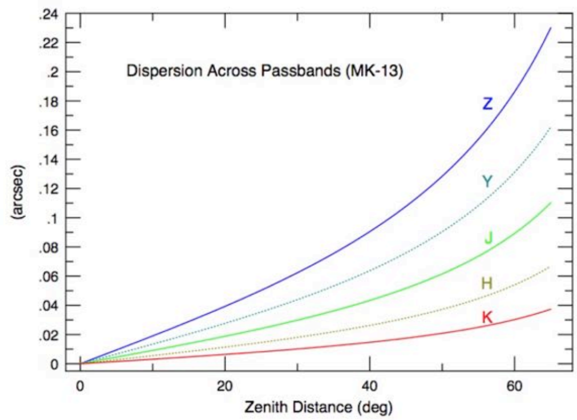

Figure 1. Atmospheric dispersion within the various passbands covered by IRIS, as a function of zenith distance. This figure shows the dispersion of the blue edge relative to the red edge of each passband. The dispersion has been calculated for the adopted site of TMT on Mauna Kea.

Phillips, A. C., et al. (2010). The Infrared Imaging Spectrograph (IRIS) for TMT: the atmospheric dispersion corrector. Society of Photo-Optical Instrumentation Engineers (SPIE) Conference Series. **7735:** 189.